

Molecular-Cling-Effect of Fluoroethylene Carbonate Characterized via Ethoxy(pentafluoro)cyclotriphosphazene on SiO_x/C Anode Materials – A New Perspective for Formerly Sub-Sufficient SEI Forming Additive Compounds

Adjmal Ghaur, Felix Pfeiffer, Diddo Diddens, Christoph Peschel, Iris Dienwiebel, Leilei Du, Laurin Profanter, Matthias Weiling, Martin Winter,* Tobias Placke, Sascha Nowak, and Masoud Baghernejad*

Effective electrolyte compositions are of primary importance in raising the performance of lithium-ion batteries (LIBs). Recently, fluorinated cyclic phosphazenes in combination with fluoroethylene carbonate (FEC) have been introduced as promising electrolyte additives, which can decompose to form an effective dense, uniform, and thin protective layer on the surface of electrodes. Although the basic electrochemical aspects of cyclic fluorinated phosphazenes combined with FEC were introduced, it is still unclear how these two compounds interact constructively during operation. This study investigates the complementary effect of FEC and ethoxy(pentafluoro)cyclotriphosphazene (EtPFPN) in aprotic organic electrolyte in LiNi_{0.5}Co_{0.2}Mn_{0.3}O || SiO_x/C full cells. The formation mechanism of lithium ethyl methyl carbonate (LEMC)-EtPFPN interphasial intermediate products and the reaction mechanism of lithium alkoxide with EtPFPN are proposed and supported by Density Functional Theory calculations. A novel property of FEC is also discussed here, called molecular-cling-effect (MCE). To the best knowledge, the MCE has not been reported in the literature, although FEC belongs to one of the most investigated electrolyte additives. The beneficial MCE of FEC toward the sub-sufficient solid-electrolyte interphase forming additive compound EtPFPN is investigated via gas chromatography-mass spectrometry, gas chromatography high resolution-accurate mass spectrometry, in situ shell-isolated nanoparticle-enhanced Raman spectroscopy, and scanning electron microscopy.


1. Introduction

Lithium-ion batteries (LIBs) have gained significant attention in the last decade. The high energy density, long lifetime, and low costs per energy content make LIBs an indispensable technology for various applications such as mobile devices and electromobility.^[1–3] Besides appropriate anode and cathode active materials, it is still a major challenge to design an electrolyte that can fulfill all the requirements like effective anode or cathode passivation, i.e., solid-electrolyte interphase (SEI) or cathode electrolyte interphase (CEI) formation, without affecting the bulk properties of the base electrolyte. Ideally, additive components decompose prior to the base electrolyte to passivate the electrodes.^[1,2] Fluorinated cyclic phosphazene compounds as film-forming additive material with beneficial passivation properties were recently reported by Liu et al.^[3] They identified a LiF-containing SEI on the anode and a phosphorous- and nitrogen-rich CEI on the cathode in an LNMO || Li metal cell using an electrolyte with this additive.^[3,4]

With this in line, we previously

A. Ghaur, C. Peschel, I. Dienwiebel, L. Du, L. Profanter, M. Winter, T. Placke, S. Nowak
University of Münster
MEET Battery Research Center
Institute of Physical Chemistry
Corrensstr. 46, 48149 Münster, Germany
E-mail: m.winter@fz-juelich.de

F. Pfeiffer, D. Diddens, M. Weiling, M. Winter, M. Baghernejad
Helmholtz Institute Münster
IEK-12
Forschungszentrum Jülich GmbH
Corrensstr. 46, 48149 Münster, Germany
E-mail: b.masoud@fz-juelich.de

 The ORCID identification number(s) for the author(s) of this article can be found under <https://doi.org/10.1002/smll.202302486>

© 2023 The Authors. Small published by Wiley-VCH GmbH. This is an open access article under the terms of the Creative Commons Attribution License, which permits use, distribution and reproduction in any medium, provided the original work is properly cited.

DOI: 10.1002/smll.202302486

investigated fluorinated cyclic phosphazene compounds in combination with fluoroethylene carbonate (FEC) as a dual-additive approach in electrolytes to foster cell stability by effective SEI formation in $\text{LiNi}_{0.5}\text{Co}_{0.2}\text{Mn}_{0.3}\text{O}_2$ (NCM523) || SiO_x/C pouch cells.^[5] Investigations on the silicon anode passivation properties at the anode side and electrochemical performance measurements have also been performed. The suppression of gas formation of the dual-additive electrolyte with fluoroethylene carbonate (FEC)/hexafluorocyclotriphosphazene (HFPN)-derivatives have been studied and electrochemical aspects of the synergistic effect between FEC and HFPN-derivatives have been discussed. Since ethoxy(pentafluoro)cyclotriphosphazene (EtPFPN) has shown the lowest cell impedance among the investigated HFPN-derivatives, this study examines the impact of the dual-additive combination FEC/EtPFPN (1:1 molal ratio) on the electrolyte and SEI composition during the initial operation of the cell with ethylene carbonate (EC)/ethyl methyl carbonate (EMC) (3/7) as solvent and 1 M lithium hexafluorophosphate (LiPF_6) as conducting salt.

Recently, Henschel et al.^[6] proposed an electrochemical decomposition route via a single-electron reduction pathway of EC, which leads to trans-esterification and formation of oligomerization products (oligo carbonates) like dimethyl carbonate (DMC), di-ethylene carbonate (DEC), ethylmethyl-2,5-dioxahexane-carboxylate (EMDOHC), dimethyl-2,5-dioxahexane-carboxylate (DMDOHC) and diethyl-2,5-dioxahexane-carboxylate (DEDOHC) hereinafter referred to as OHCs. These OHCs are associated in the literature with gas generation and capacity loss in the initial charging process.^[7–11] Hence, deteriorating electrochemical performance leading to increased impedance growth is correlated with these species due to increased interphase layer formation.^[6,7,12] Henschel et al.^[6] subdivided the OHC formation into three stages; i) the initiation, ii) the elongation, and iii) the termination stage, starting with the formation of the intermediate compound lithium ethyl methyl carbonate (LEMC) via a single electron reduction of EC in the initiation stage. Gachot et al.^[9] proposed prior to Henschel et al. the same compound (LEMC) and called it Intermediary A. However, Gachot et al.^[9] proposed a nucleophilic lithium alkoxide attack on EC as the initial reaction, which led to the formation of LEMC via a ring-opening reaction of EC. In both reaction pathways, LEMC is mentioned as the origin of the formed OHCs.

Considering the proposed OHCs formation mechanisms by Henschel et al.^[6] and Gachot et al.,^[9] as well as the electrochemical observations in terms of long-term performance, gas evolution, and electrode passivation properties with FEC/HFPN-derivatives as dual-additive electrolyte compounds in our previous study, it is likely that there is a correlation between the improved electrochemical performance with the dual-additive electrolyte approach, the LEMC intermediate compound, and the observed reduced OHC formation.^[5] Especially the role of lithium alkyl carbonates like lithium ethyl carbonate (LEC) and LEMC are mentioned to be essential for the formation of such effective SEI. LEMC as EC reductive decomposition product facilitates a relatively high Li^+ conductivity ($>1 \times 10^{-6} \text{ S cm}^{-1}$) and is mentioned as the main SEI constituent by Wang, Xu, Eichhorn, and colleagues.^[13] LEC, as the reductive decomposition product of EMC and DEC, is involved in the SEI formation as a precursor for the formation of lithium carbonate (Li_2CO_3), car-

bon dioxide (CO_2), lithium fluoride (LiF) and difluorophosphate ($\text{LiF}_2\text{O}_2\text{P}$).^[14,15]

To better understand the influence of these compounds in SEI formation, this study analyzes the synergistic effect of EtPFPN and FEC as electrolyte additives in NCM523 ($\text{LiNi}_{0.5}\text{Co}_{0.2}\text{Mn}_{0.3}\text{O}_2$) || SiO_x/C pouch cells to understand their interaction with other electrolyte constituents in terms of SEI formation and improvement of electrochemical performance, to shed light on the reactions behind OHC formation.^[6] Furthermore, the role of lithium alkoxide as an EC ring opening initiator during initial OHC formation is explored in this context.^[9] Finally, the contribution of FEC toward improving the electrochemical performance is discussed, and the specific effect of molecular clinging – (defined here as molecular-cling-effect, abbreviated MCE) of FEC will be introduced. The proposed reaction mechanisms at the electrode|electrolyte interface is backed up with post-mortem and in situ investigations. The MCE of FEC will be verified and explained via gas chromatography-mass spectrometry, gas chromatography high resolution-accurate mass spectrometry (GC-MS), gas chromatography-mass spectrometry, gas chromatography high resolution-accurate mass spectrometry (GC-HRMS) measurements of the liquid electrolyte, and via in situ shell-isolated nanoparticle-enhanced Raman spectroscopy (SHINERS) measurements at the electrode|electrolyte interface.^[16–18] Finally, scanning electron microscopy (SEM) investigations have been performed to visualize the morphological difference between the benchmark electrolyte (EC/ethyl methyl carbonate (EMC) 3:7, 1 M LiPF_6 , referred here as to standard, STD) STD-FEC and the dual-additive electrolyte blend STD-FEC-EtPFPN after SEI formation.

2. Results and Discussion

2.1. Electrochemical Performance of Dual-Additive-Based LIB Full Cells

NCM523 || SiO_x/C multilayered pouch cells (with 10 wt.% SiO_x) were charged/discharged for 200 cycles. The specific capacities of all cells containing different electrolyte formulations (see Table 2 for details) were normalized to that of the first discharge cycle after the SEI formation (third cycle). The normalized discharge capacity of the cells and the difference between the mean charge and the mean discharge voltage (ΔV) is plotted for the STD (1 M LiPF_6 in EC:EMC 3:7 by wt.), STD-FEC (2 wt.% FEC), and the STD-FEC-EtPFPN (FEC/EtPFPN 1:1 molal ratio) electrolytes (Figure 1A,B). Further electrochemical investigations (e.g., long-term performance, gas generation, self-discharge) regarding HFPN-derivatives as electrolyte additives in NCM523 || SiO_x/C multilayered pouch cells (with 10 wt.% SiO_x) have been discussed in our previous study.^[5]

The ΔV plot shows the difference between the mean charge and the mean discharge voltages. These can give an estimation of the cell polarization upon (dis)charging and can be correlated to the cell impedance of different electrolyte blends upon cycling.^[19,20] Cells using the STD and the STD-EtPFPN electrolyte formulation show the lowest ΔV value after the first formation cycle. On the flip side, the ΔV value of the cells containing the STD electrolyte blend increases after ≈ 50 cycles (dashed black line), and for cells containing the STD-EtPFPN electrolyte

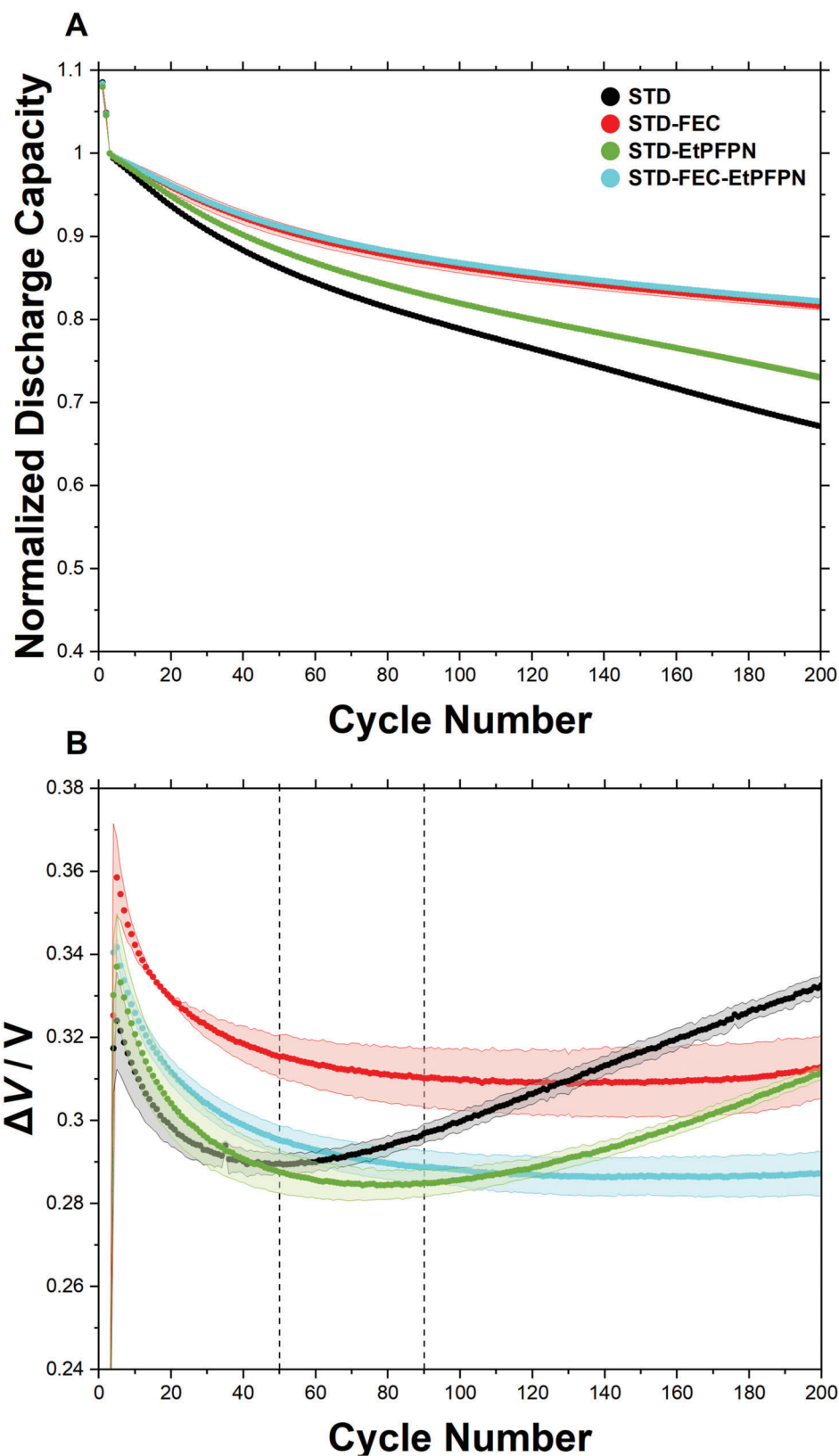


Figure 1. A) Electrochemical measurements at 20 °C during long-term cycling (2.8 V – 4.3 V at 100 mA (≈ 0.5 C)) in NCM523 || SiO_x/C pouch cells for different electrolyte formulations: normalized discharge capacity, and B) cell polarization (ΔV) versus cycle number. STD-FEC electrolyte blend is a state-of-the-art electrolyte formulation.

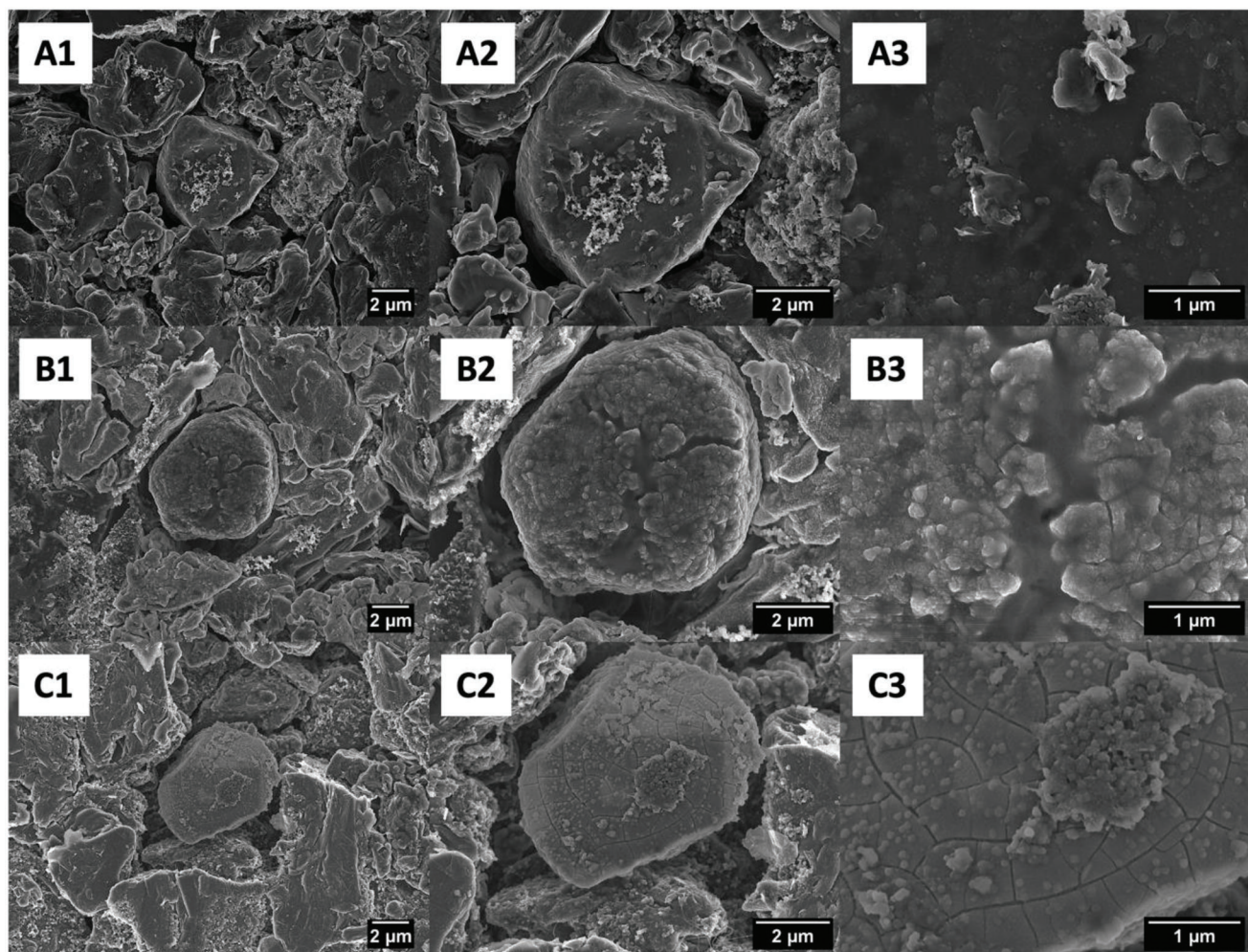


Figure 2. A1–A3) SEM images of the pristine Si particle state. B1–B3) SEM images after SEI formation with the benchmark STD-FEC electrolyte blend. C1–C3) SEM images after the SEI formation with the STD-FEC-EtPFPN electrolyte blend.

formulation, the ΔV value increases after ≈ 90 cycles compared to the STD-FEC and the STD-FEC-EtPFPN electrolyte blends. Two reasons can be assumed to be responsible for this behavior, which are i) formation of an ineffective SEI on the anode surface and ii) silicon volume changes upon (dis)charging, resulting in continuous electrolyte decomposition on the anode surface upon cycling.^[21–23] The dual-additive electrolyte approach using FEC and EtPFPN shows the most promising SEI formation properties and cycling performance of up to ≈ 200 cycles among the four investigated electrolytes. The highest ΔV value, hence, the highest cell impedance, in the initial stage (SEI formation), is observed for the STD-FEC electrolyte blend; after SEI formation. Thus, a more resistive SEI formation is indicated, since FEC is an effective SEI-forming additive for Si-based cells.^[21,24] To obtain a better understanding of the SEI morphology, SEM images have been acquired from the pristine Si particle surface (Figure 2, A1–A3) and after SEI formation in the STD-FEC (Figure 2, B1–B3) and in the STD-FEC-EtPFPN electrolyte blends (Figure 2, C1–C3), respectively.

As can be seen in Figure 2, SEI formation can be detected for both electrolyte formulations in Figure 2 (B1–B3, C1, C2) com-

pared to the pristine state (Figure 2, A1–A3). The STD-FEC electrolyte blend results in a more inhomogeneous surface morphology with huge Si particle cracks, while the dual-additive approach (STD-FEC-EtPFPN) shows a more homogeneous surface morphology with thin cracks on the anode surface, which are not progressing after SEI formation. Considering the initial results in the ΔV plot, showing the highest initial ΔV value for the STD-FEC electrolyte blend upon cycling, it can be stated that an improved SEI formation takes place on the anode surface in the presence of STD-FEC-EtPFPN.

The ΔV plot and the SEM images indicate a trend toward a better anode passivation behavior for the dual-additive electrolyte formulation. Since the SEI formation process is dependent on the electrolyte composition, it can be assumed that a synergistic effect of FEC and EtPFPN during this process takes place. Inevitably, this leads to a more homogenous SEI morphology compared to the benchmark electrolyte blend. To better understand these multi-molecular compound interactions in the initial SEI formation process, the decomposition/aging products of the different electrolyte blends at the anode|electrolyte interface have been analyzed.

2.2. Electrolyte Analysis via Gas Chromatography-High Resolution Mass Spectrometry

To analyze the electrolyte decomposition/aging products, GC-MS and GC-HRMS measurements have been performed after the SEI formation. According to the electrochemical results in Figure 1, the SEM images in Figure 2, and the results of our previous study,^[5] it can be assumed that EtPFPN decomposition takes place along with other electrolyte components like FEC, EC, and EMC on the negative electrode surface during the SEI formation.^[5] The decomposition products after SEI formation have been analyzed to prove this assumption indirectly. As indirect proof, trans-esterification and oligomerization products like OHCs from EC decomposition or increased DMC/DEC formation from EMC decomposition in the aged electrolyte during SEI formation would be expected.^[7,13,25–29] It is worth mentioning that these decomposition products are resulting from parasitic reactions deteriorating electrochemical performance and lead to increased impedance growth. In turn, inhibiting the formation of these species would be beneficial for electrochemical performance.^[6,7,12] In **Figure 3**, the decomposition of each investigated electrolyte blend can be observed after the SEI formation step. In contrast to the STD electrolyte blend in **Figure 3B**, the cells with STD-FEC, STD-EtPFPN, and STD-FEC-EtPFPN in **Figure 3A** show decreased amounts of DMC and DEC and all the other OHCs. The results are in good agreement with the previous study of our group and with observations discussed in the literature concerning film-forming additives like FEC, VC, and HFPPN-derivatives at the negative electrode or the formation of OHCs via trans-esterification upon cycling.^[6,10,30,31] Interestingly, reduced Li-alkoxide generation associated with the formation of DEC in the aged electrolyte has also been confirmed. Thus, a reduced DEC formation means indirectly that Li-alkoxide formation is also reduced.^[6]

A second notable observation in the GC-MS chromatogram in **Figure 3A** is the EtPFPN decomposition in the STD-FEC-EtPFPN electrolyte blend compared to the STD-EtPFPN electrolyte blend after SEI formation. No EtPFPN decomposition products are detectable in the STD-FEC-EtPFPN blend compared to the chromatogram for the STD-EtPFPN electrolyte blend; thus, one would expect EtPFPN decomposition in the STD-FEC-EtPFPN electrolyte blend, as well. The question that appears at this point is, where are the EtPFPN decomposition products that one would expect in the STD-FEC-EtPFPN electrolyte blend, considering that EtPFPN consumption takes place according to the GC-MS chromatogram of the STD-EtPFPN electrolyte formulation? Furthermore, FEC consumption takes place in the STD-FEC and the STD-FEC-EtPFPN electrolyte blends after SEI formation.

To better understand the EtPFPN decomposition products, GC-HRMS measurements of the liquid electrolyte have been performed to determine the chemical structure of the EtPFPN decomposition products upon SEI formation and to trace back their formation. The different EtPFPN decomposition species are illustrated in **Figure 4** and the corresponding evaluated GC-HRMS data are presented in **Figures S1 and S2** (Supporting Information).

The absence of EtPFPN decomposition peaks in the GC-MS of the STD-FEC-EtPFPN electrolyte blend (**Figure 3**) after SEI for-

mation is notable since EtPFPN as a single additive compound without FEC is not known as an effective SEI forming additive for SiO_x/C based anode materials, but rather as electrolyte stabilizing agent at high temperatures (60 °C).^[5] Recently, Liu et al.^[4,32] demonstrated in LiNi_{0.5}Mn_{1.5}O₄ (LNMO) || Li metal cells that EtPFPN as a single-additive electrolyte compound contributes to the formation of a beneficial LiF-rich SEI and generates a dense, uniform, thin, and phosphorous- and nitrogen-rich CEI layer on the surface of LNMO at high cell voltages (> 4.5 V). However, in their study^[4] EtPFPN decomposition product traces have only been found on the cathode side, but not on the anode side (Li-metal). In our previous study using NCM523 || SiO_x/C multi-layered pouch cells (with 10 wt.% SiO_x), an ineffective SEI formation for SiO_x/C electrodes has been observed for EtPFPN as a single-additive electrolyte compound.^[5] In contrast, a more effective SEI has been observed when combining FEC and EtPFPN through a dual-additive electrolyte approach (STD-FEC-EtPFPN). Likely, the EtPFPN decomposition product accumulation occurs on the negative electrode surface during the SEI formation process in the single-additive approach (STD-EtPFPN). However, it seems that these species are not able to participate effectively in the SEI formation as SEI constituents. Therefore, these species are not able to cling effectively as SEI constituents. This explains the LiF-rich SEI mentioned by Liu et al. without EtPFPN decomposition product traces on the anode surface.^[3,4] Considering the large volume expansion of the Si-particles (≈300%) happening continuously during the (de)lithiation process, along with particle cracking and thereby notable capacity fading, the importance of an additive ability to cling on the surface of the negative electrode to maintain a sufficient SEI is highlighted.^[33,34]

To better understand SEI formation and FEC/EtPFPN interaction, the EtPFPN decomposition products have been elucidated via GC-HRMS (**Figure 4, 1a–d**). Based on i) the analytical results (**Figures 3 and 4**) and ii) the lithium alkoxide-initiated ring opening of EC to non-symmetric lithium carbonate LEMC (Intermediary A) proposed by Gachot et al.,^[9] it was possible to propose a reaction mechanism that can explain the analytical observations in **Figures 3 and 4** regarding the reaction between EtPFPN and LEMC (Intermediary A). Since LEMC is the origin of OHCs and OHC formation has been notably reduced in the STD-EtPFPN electrolyte blend, a causal relation between EtPFPN and LEMC is assumed. In turn, this leads to the notably reduced OHC formation in **Figure 3**. The GC-HRMS data for the STD-EtPFPN electrolyte blend after SEI formation in **Figure 4** indicates a reaction between EtPFPN and LEMC. The reaction mechanism of LEMC with EtPFPN to the different compound derivatives 1c–1d (hereafter referred to as EtPFPN-LEMC species) is proposed in **Figure 5A**.

The scheme in **Figure 5A** illustrates the nucleophilic addition of lithium alkoxide to the electrophilic C=O carbon atom of cyclic EC, followed by a ring opening to the non-symmetric linear lithium alkyl carbonate (LEMC/Intermediary A). Since EC has a planar symmetric structure and no chiral carbon atoms, the nucleophilic attack can occur from both faces (re and si face) without specific preference. According to Gachot et al.,^[9] in the following step a preferred nucleophilic attack from the newly formed LEMC with linear carbonates (i.e., DMC, EMC, DEC) is expected to form OHCs.^[6,9] Since the electrolyte solvents in this study are EC and EMC, two different LEMC (Intermediary A)

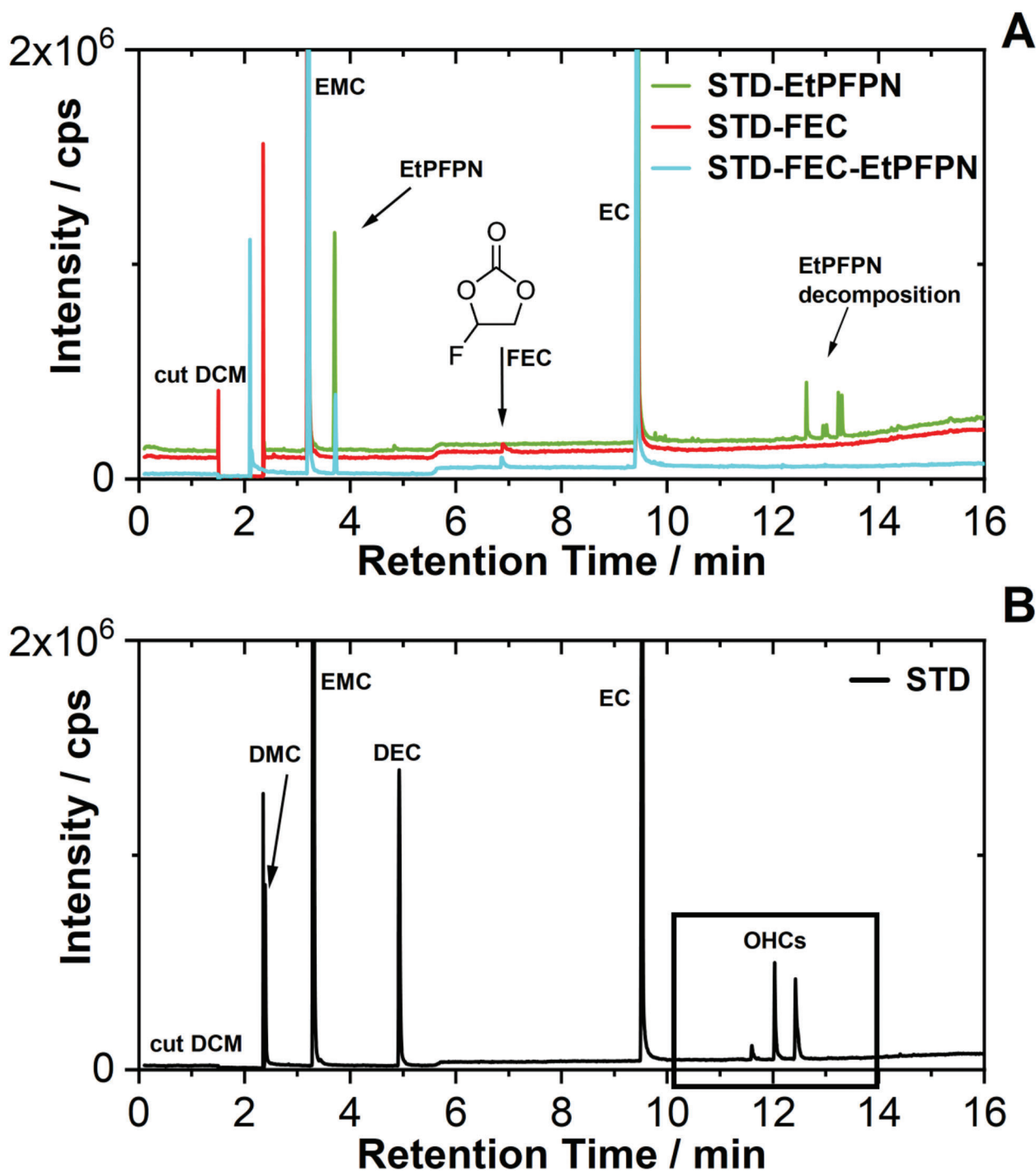
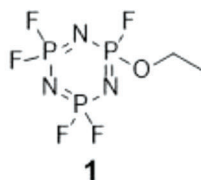


Figure 3. GC-MS of different extracted electrolyte blends after SEI formation, as shown in the insert. A) The entire chromatograms for the STD-FEC blend, the STD-EtPFPN blend, and the STD-FEC-EtPFPN blend. B) The entire chromatogram for the STD electrolyte. Please note that artificial signals at (2.10 and 2.34) originated after the solvent cut for DCM caused by reestablishing the filament voltage, and need to be not mixed up with the DMC signals, which are occurring at longer retention times.

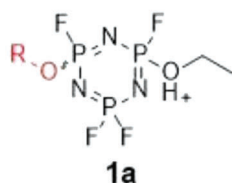
structures with R = methyl (Me) or ethyl (Et) are shown in Figure 5. Based on the GC-MS results (Figure 3), DMC formation is notably reduced in the electrolytes containing STD-EtPFPN and STD-FEC-EtPFPN.^[5] Therefore, the equilibrium between cyclic EtPFPN and DMC is favored toward the reac-

tion of LEMC with EtPFPN instead of the proposed reaction suggested by Gachot et al.,^[9] where a nucleophilic reaction between LEMC and DMC was proposed, leading to the formation of OHCs (blue arrow in Figure 5A). Hence, a higher concentration of cyclic EtPFPN in the electrolyte than DMC favors

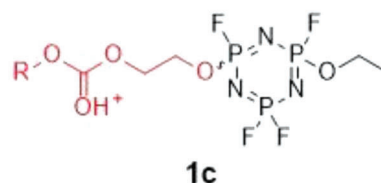
Targeted cyclic EtPFPN species



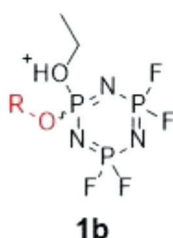
Identified characteristic $[M+H]^+$ adducts of cyclic EtPFPN



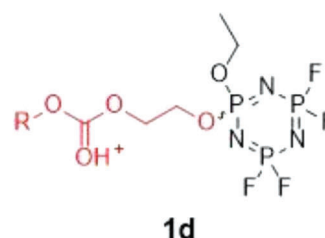
R = Me Exact Mass: 287.9838
R = Et Exact Mass: 301.9995
Figure S1.



R = Me Exact Mass: 375.9999
R = Et Exact Mass: 390.0155
Figure S2



R = Me Exact Mass: 287.9838
R = Et Exact Mass: 301.9995
Figure S1.



R = Me Exact Mass: 375.9999
R = Et Exact Mass: 390.0155
Figure S2

Figure 4. Fragment ions of EtPFPN in the STD-EtPFPN electrolyte blend after SEI formation identified via GC-HRMS; the corresponding GC-HRMS spectra are shown in Figures S1 and S2 (Supporting Information). Ortho substituted side-groups upon nucleophilic addition are marked in red.

the proposed reaction path between LEMC and EtPFPN. However, as EMC is used as the main electrolyte solvent, a nucleophilic reaction between LEMC and EMC, leading to the formation of OHCs, would be expected. Interestingly, in both blends (STD-EtPFPN, STD-FEC-EtPFPN), a notably reduced OHC formation has been detected after SEI formation. Hence, a more favored reaction between LEMC and EtPFPN than the reaction with DMC, DEC, and/or EMC is indicated. The preferred nucleophilic addition of LEMC with EtPFPN occurs through a transition state, as proposed in Figure 5A,B, where it is assumed that Li^+ coordination takes place prior to the nucleophilic attack of LEMC on the EtPFPN ring structure.^[35,36] By interpretation of NMR data, Luther et al.^[35] postulated polyphosphazene Li^+ coordination in the pocket-like structures with the nitrogen nuclei and functional groups at the phosphorus entity. Benson et al.^[36] used Density Functional Theory (DFT) results to suggest the same Li^+ coordination in pocket-like structures in the cyclic phosphazene backbone, whereas similar observations have been made for polyphosphazene in ref. [37] According to this study, it can be assumed that Li^+ coordination in the pocket-like structures leads to a ring-opening of EtPFPN, which accelerates LiF

release. Since EtPFPN possesses two different *ortho*-substituted side groups in the ring structure (PF_2 and PFOEt), two possible reaction mechanisms have been proposed. In the reaction pathway of Figure 5A, LiF is produced as a side product upon this reaction path, leading to EtPFPN-LEMC derivative compounds, which are identified in GC-HRMS measurements of the STD-EtPFPN electrolyte blend after SEI formation (Figure 4,1c–d). The second mechanism in Figure 5B illustrates the reaction after LEMC formation as described in Figure 5A and, therefore, starts with the transition state, where a nucleophilic attack of LEMC with the EtPFPN-core structure is suggested. In contrast to the reaction pathway in 5A, in pathway 5B lithium alkoxide (EtOLi) is proposed as a side product instead of LiF within the formation of the compound 1e (hereafter referred to as PFPN-LEMC species) (Figure 5B,1e). To determine which reaction pathway is more favored and to better understand the reaction process, DFT calculations regarding the release of LiF and EtOLi have been performed for both reaction pathways at 298 K (Figure 6A,B). These result in a thermodynamically more favored LiF release after nucleophilic addition of LEMC to EtPFPN ($\Delta G = -21.3 \text{ kcal mol}^{-1}$, $\Delta E = -25.2 \text{ kcal mol}^{-1}$ at the $\omega\text{B97X-D3/def2-TZVP}$

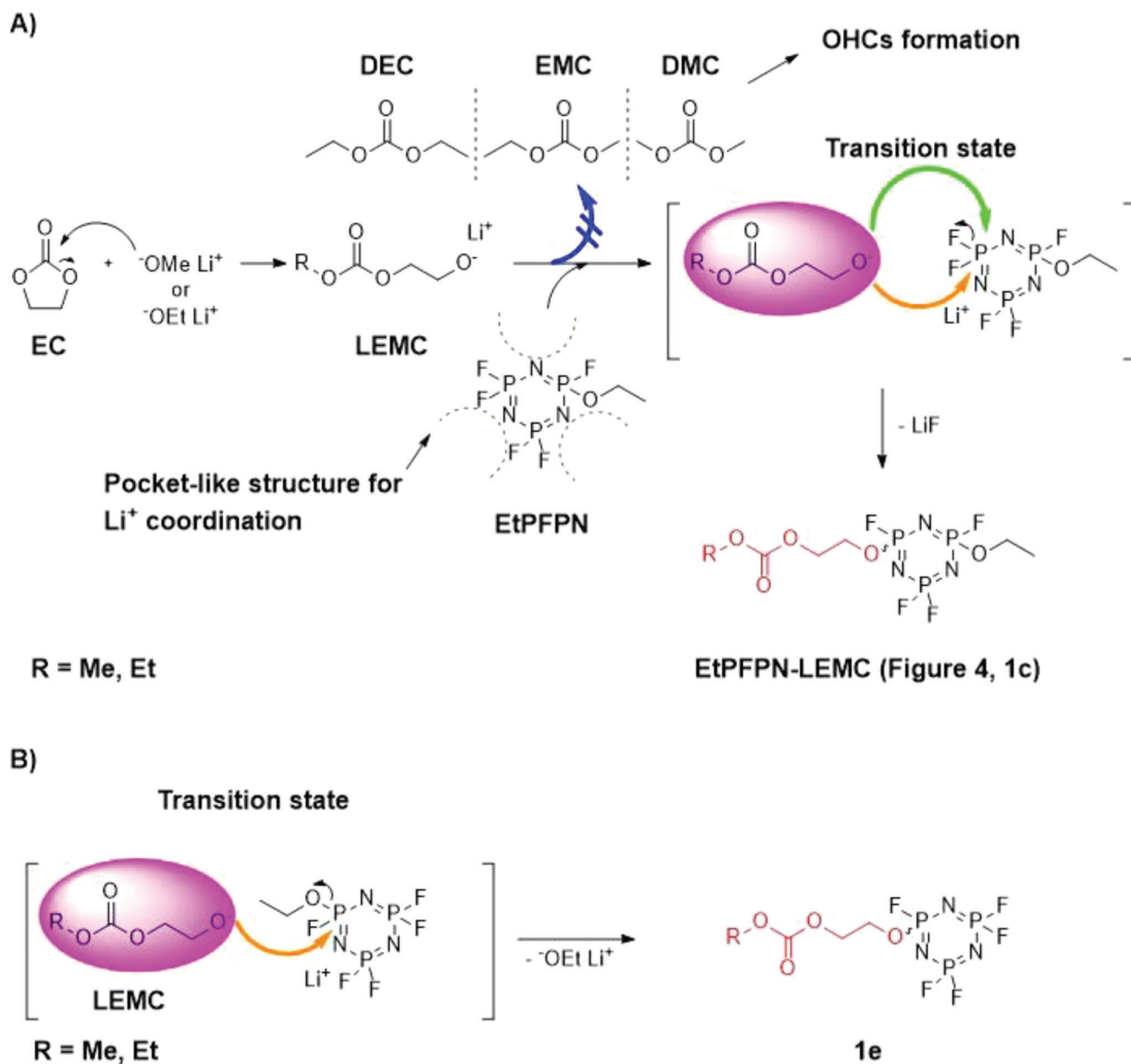


Figure 5. Proposed reaction mechanism of LEMC with EtPFPN. The blue arrow shows the inhibited reaction mentioned by Gachot et al.^[9] The pocket-like Li^+ coordinating structures of EtPFPN, according to Luther et al.^[35] is marked with brown dashed lines. A) A nucleophilic attack of LEMC (pink ellipse) is proposed from the re and se side (orange arrow and green arrow) in the transition state; B) a nucleophilic attack of LEMC (pink ellipse) is proposed (orange arrow) in transition state, which due to steric effects of the bulky ethoxy side group happens in ortho-position.

level of theory^[38–41] for compound 1c). In contrast, lithium alkoxide (OEtLi) release from the EtPFPN core structure after the nucleophilic addition of LEMC is thermodynamically less favored ($\Delta G = 5.1 \text{ kcal mol}^{-1}$, $\Delta E = 4.6 \text{ kcal mol}^{-1}$ for compound 1d). Additionally, DFT calculations for the LiF release have been done for the ipso-structure of the EtPFPN-LEMC species after nucleophilic reaction of LEMC with EtPFPN (Figure 6A, 1d). This compound has also been observed via GC-HRMS measurements of the STD-EtPFPN electrolyte blend and has a thermodynamically exergonic LiF release according to the DFT calculations ($\Delta G = -20.7 \text{ kcal mol}^{-1}$, $\Delta E = -24.6 \text{ kcal mol}^{-1}$ for compound

1d). However, considering that the EtPFPN structure has two PF_2 moieties and only one PFOEt constituent, a higher probability toward the reaction leading to compound derivative 1c, which is thermodynamically slightly more favored compared to compound 1d, can be assumed. Interestingly, these computed energy values with a high driving force for LiF release confirm experimental results regarding an increased LiF formation by Liu et al.^[3,4]

These computed energy values are in good agreement with the identified GC-HRMS structures in Figure 4, 1c–d. Thus, all thermodynamically exergonic reaction products have been confirmed

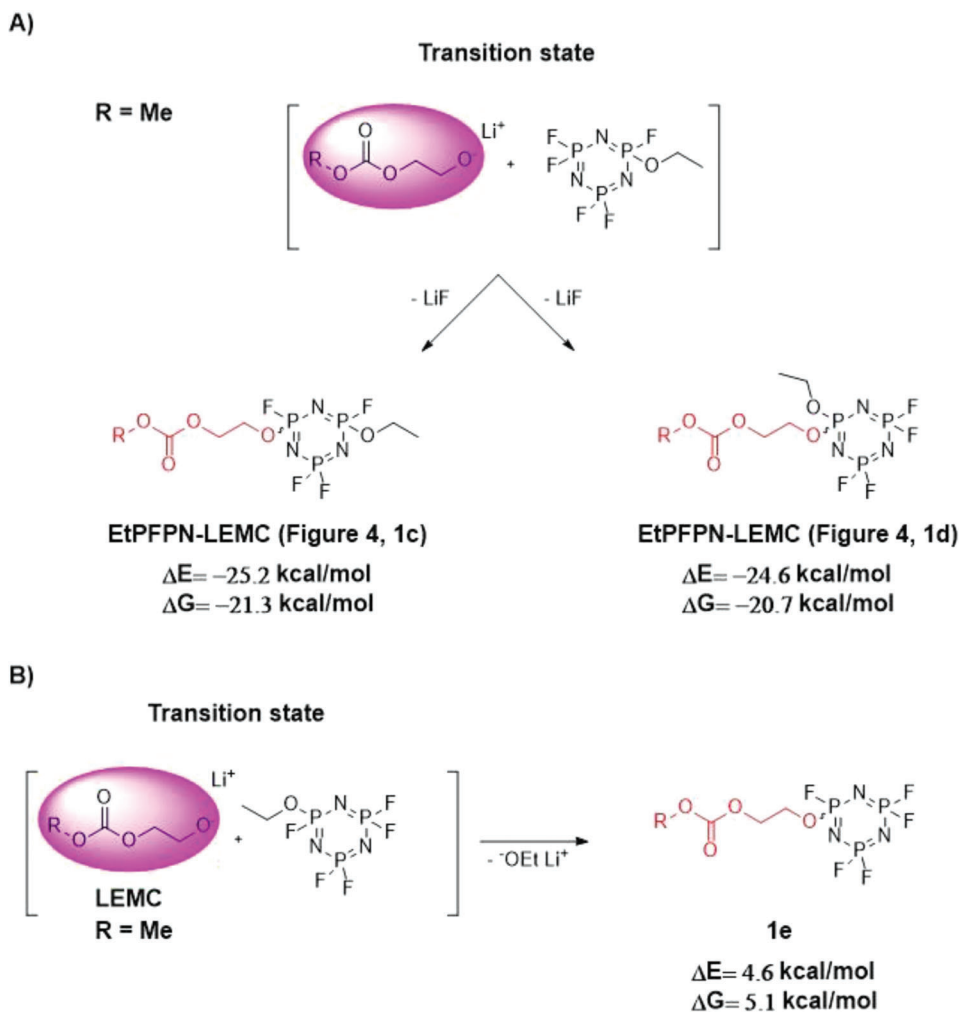


Figure 6. Computed thermodynamic calculation of A) LiF and B) lithium alkoxide release upon the nucleophilic reaction of LEMC species with EtPFPN.

via GC-HRMS measurements, while the endergonic reaction products have not been validated via GC-HRMS.

Comparing both reaction pathways 5A and 5B, a preferred reaction through pathway 5A is assumed since it is thermodynamically favorable. On the flip side, the endergonic reaction path in 5B can be neglected. In addition to the proposed reaction mechanism in Figure 5A, which leads to the EtPFPN-LEMC compound derivatives 1c-1d, a competing reaction is proposed in terms of lithium alkoxide compounds (LiOMe, LiOEt), which can react directly with the EtPFPN ring structure via a nucleophilic addition as schematically shown in Figure 7A,B. This reaction results in LiF as a side product and leads to the formation of the identified molecular structure in the GC-HRMS data of the STD-EtPFPN electrolyte blend (Figure 4, 1a-b). The DFT calculations for LiF release upon a nucleophilic reaction of the lithium alkoxide species with EtPFPN show again an exergonic reaction process ($\Delta G = -26.0 \text{ kcal mol}^{-1}$, $\Delta E = -27.6 \text{ kcal mol}^{-1}$ for compound 1a upon a reaction of EtPFPN with LiOMe; and $\Delta G = -25.8 \text{ kcal mol}^{-1}$, $\Delta E = -28.2 \text{ kcal mol}^{-1}$ for compound 1b upon a reaction of EtPFPN with LiOEt). The computed results also agree with the GC-MS measurements in Figure 3. Thus, EtPFPN can

react with LEMC and lithium alkoxide to the observed GC-HRMS structures via an exergonic LiF release.

Therefore, it is assumed that a reduced reaction between lithium alkoxide and EC through a nucleophilic attack of lithium alkoxide species takes place, which is in agreement with the exergonic lithium alkoxide reaction with EtPFPN (Figure 7), the endergonic lithium alkoxide release from EtPFPN (Figure 6B), and findings of Gachot et al.^[9] Overall, these influences of EtPFPN, also in combination with FEC, lead to notably reduced EC decomposition reactions, hence, reduced side reactions, OHC formation, and gas evolution, which supports the proposed reaction mechanism in Figure 5A and previous experimental results by our group.^[5,7]

To obtain a better understanding of the compound structures after nucleophilic reaction of LEMC or lithium alkoxide with EtPFPN 1, minimum energy structures of the complex geometries have been computed according to the Conformer Rotamer Ensemble Sampling Tool (CREST) by Grimme, Pracht, Banwarth, and colleagues (Figure 8).^[42,43] According to these computed structures and the thermodynamic driving force regarding LiF release. It is feasible for the PF_2 moieties of EtPFPN

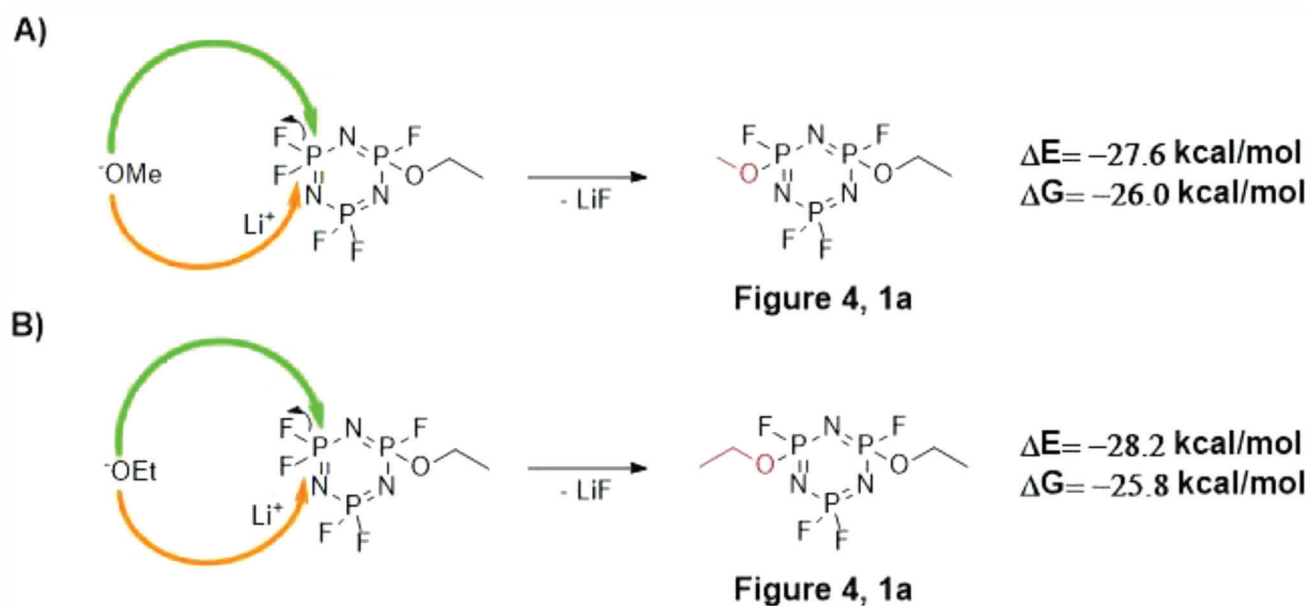


Figure 7. Proposed reaction mechanism of the lithium alkoxide species with the EtPFPN ring structure. Nucleophilic addition of lithium alkoxide from both sides (re and se) is possible (green and orange arrow) in both cases (A) and (B).

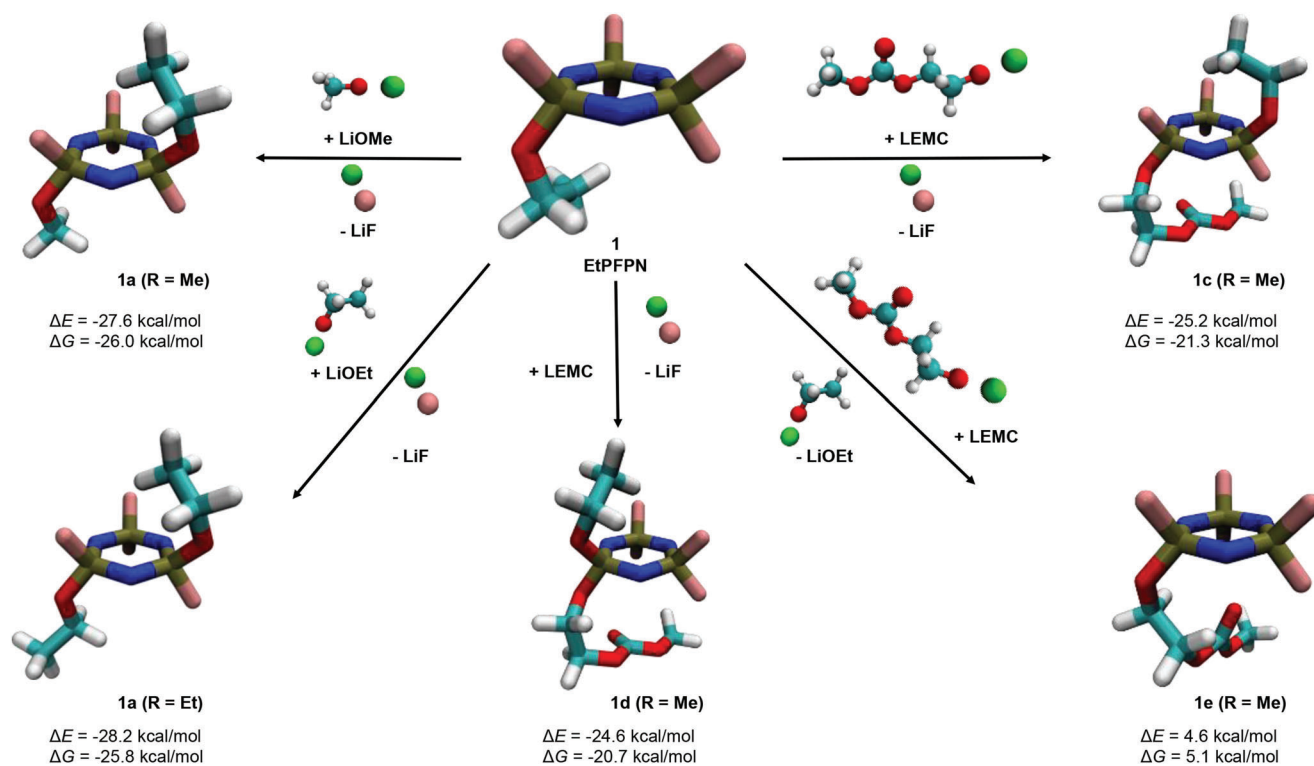


Figure 8. Computed minimum energy structures of the identified compounds in the GC-HRMS measurements via CREST, which were subsequently reoptimized at the ω B97X-D3/def2-TZVP level of theory, at which also the reaction (free energies) were computed. Nitrogen (N, dark blue); fluoride (F, pink); phosphorus (P, dark green); oxygen (O, red); carbon (C, light blue); hydrogen (H, white); lithium (Li, green).

to undergo further reactions. However, in the GC-HRMS measurements after the SEI formation, only the identified $[M+H]^+$ adducts in Figure 4 were observed for the STD-EtPFPN electrolyte blend. A higher LEMC or lithium alkoxide formation during the SEI formation could lead to further reactions with not reacted PF_2 moieties of the EtPFPN compound, and, thus, to new $[M+H]^+$ adducts via GC-HRMS.

In summary, with the reaction pathways described herein, a lower net outcome of side products can be stated, compared to the OHC formation reaction described by Henschel et al.^[6] Thus, this finding agrees with the electrochemical results regarding lower cell resistance values for the STD-FEC-EtPFPN electrolyte blend (Figure 1) due to lower parasitic side reactions, which are a secondary effect of side products starting with the elongation process as described by Henschel et al.^[6] Both proposed reaction mechanisms (Figures 5A and 7A,B) are possible pathways. However, besides the thermodynamic effect in the transition state, both are dependent on the mass equilibrium between LEMC formation and the presence of EtPFPN. Considering that i) EC is the main component of the electrolyte next to EMC, and ii) that LEMC is a product of EC decomposition as schematically proposed in Figure 5A, it is assumed that the reaction mechanism proposed in Figure 5A is the more favored reaction pathway instead of the direct reaction of lithium alkoxide species with the EtPFPN ring structure in Figure 7. Since the concentration of EtPFPN as an electrolyte additive is much lower compared to the concentration of EC as a solvent, the probability is lower that the reaction takes place according to the proposed scheme in Figure 7. Instead, it is rather possible that lithium alkoxide reacts with EC to form LEMC. However, the reaction path in Figure 7 still cannot be neglected, as suggested by the GC-HRMS results in Figure 4,1a-b. Considering that LiF is the main side product in the proposed reaction mechanisms in Figure 5A and Figure 7A,B, one can expect a higher LiF precipitation during SEI formation compared to the STD electrolyte formulation without EtPFPN, which is described in the literature by Liu et al.^[3] for the SEI formation on Li metal. Summing up, the causal relationship between EC, EMC, LEMC, lithium alkoxide, and EtPFPN has been elucidated and could be confirmed with analytical data. Additionally, the formation of a P-O bond by substituting one P-F bond has been observed. Remarkably, the formed EtPFPN decomposition species (Figure 4) include typical reactive species described for reductive EC/EMC decomposition.^[6,9] The electrochemical EC/EMC decomposition cannot be prevented during cell formation, but preferred fluorine substitution of the EtPFPN core structure by typically formed carbonate-based reactive species (LEMC, lithium alkoxide) can avoid ongoing linear and cyclic carbonate decomposition based on secondary chemical reactions, as described by Gachot et al. and Henschel et al.^[6,9]

2.3. Identifying Characteristic EtPFPN Surface Species via In Situ SHINERS of the SEI

SHINERS, an in situ surface-sensitive technique was employed to obtain a deeper interfacial molecular understanding of the SEI formation and composition. SHINERS technique benefits from its high surface sensitivity and enhancement of near-field Raman

spectroscopy by implementing core-shell plasmonic nanoparticles to the surface of the electrodes. For more information on the technical and fundamental aspects of the SHINERS technique, the reader is kindly referred to the following references.^[44–46] The in situ SHINER spectra comparison of the four electrolyte formulations in Figure 9 (Raman peak fitting of the in situ SHINERS spectra is shown in Figure S3, Supporting Information) indicates notable differences between the recorded spectra features. In summary, EtPFPN-related multiple characteristic vibrational bands have been identified on the anode surface for the STD-FEC-EtPFPN blend upon SEI formation, which indicate EtPFPN deposition. These results were confirmed with the in situ Raman measurements and other relevant previous studies.^[47,48]

spectra were collected at 532 nm (laser power 0.61 mW, $t_{acq} = 50$ s) with a 600 line/mm grating. For electrochemical aging, three cyclic voltammetry (CV) cycles in a voltage range of 2.8 – 4.3 V with a scan rate of $150 \mu V s^{-1}$ were performed using an Autolab Battery Tester (Metrohm) controlled by NOVA 2.1 (Autolab) software. EtPFPN wavenumbers are marked with dashed lines (orange). LEC/LEMC wavenumbers are marked with dashed lines (purple). All other distinct peaks are marked with dashed lines (black).

Furthermore, the in situ SHINER spectra indicate bands that can be assigned to electrode or electrolyte components. Additionally, specific bands ≈ 384 and 404 cm^{-1} , which can be assigned to LiOH and LiF, were observed for all spectra. Compared to the other investigated electrolyte formulations, the LiF band in the STD-FEC-EtPFPN electrolyte blend is slightly more distinct at 404 cm^{-1} . Nevertheless, especially for the spectra of the electrode surface cycled with the STD-FEC-EtPFPN electrolyte blend, many additional vibrational bands in contrast to the other three electrolyte formulations (STD, STD-FEC, STD-EtPFPN) have been observed. This indicates enhanced deposition of cyclic phosphazene compounds on the negative electrode surface. For instance, these bands were observed $\approx 250, 293, 445, 510, 545, 585, 700, 750$, and 947 cm^{-1} and can be assigned to active vibrations of the cyclic phosphazene, such as ring breathing or ring stretching, and the substituents. A comprehensive band assignment can be found in Tables S1–S4 (Supporting Information). Interestingly, the crystalline silicon (c-Si) peak in the STD-FEC-EtPFPN electrolyte blend is notably less distinctive than the c-Si band of the other electrolyte formulations. According to this observation, we suppose a uniform, dense passivation of the anode surface. Thus, Si particle passivation upon SEI formation influences the electrochemical performance and prevents deep penetration of the exciting laser into the electrode material. In addition, unique distinct bands at 627, 639, and 1009 cm^{-1} have been observed for the STD-FEC-EtPFPN electrolyte blend (Table S1, Supporting Information). According to the SHINERS investigations by Gajan et al.^[49] these peaks can be assigned to lithium ethyl carbonate (LEC) and LEMC.^[49] As previously discussed, Gachot et al.^[9] proposed EC as the origin of these LEMC species (Intermediary A), which is initiated by a nucleophilic attack of the Li-alkoxide species with the electrophilic carbon atom ($C=O$) of the EC ring structure. Beyond, Henschel et al.^[6] proposed a single-electron reduction of EC which can also lead to LEMC as an intermediate compound, reacting further to OHCs via an elongation and termination step. Additionally, Xu et al.^[50] postulated LEC as a reduction product from EMC. However, this accounts for the fact

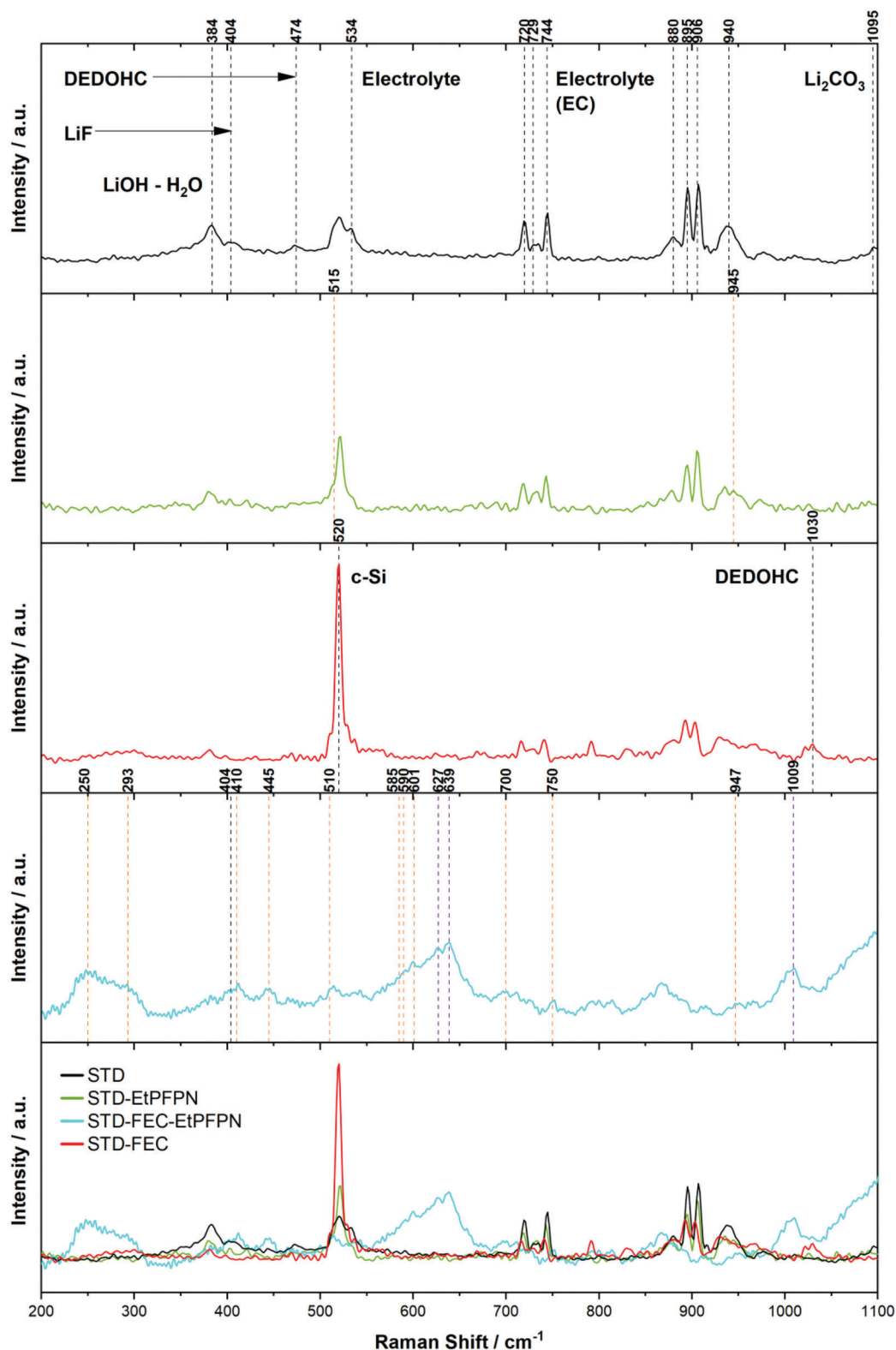


Figure 9. In situ shell isolated enhanced Raman spectroscopy (SHINERS) of the SEI composition on SiO_x/C-based negative electrodes in an EC/EMC (3/7), LiPF₆ (1 M) electrolyte environment (STD) with different additive compositions. Raman.

that EC and EMC are the main components of the electrolyte solvent used in this study.^[10] In this line, the GC-HRMS evaluation of the STD-EtPFPN electrolyte blend after the SEI formation confirms the reaction between EtPFPN and LEMC to the EtPFPN-LEMC species (Figure 4,1c). Interestingly, only two characteristic EtPFPN vibration bands (515 and 945 cm^{-1}) have been detected and verified via in situ Raman measurements of the anode surface for the STD-EtPFPN electrolyte blend during the SEI formation (Figure 9, Table S2, Supporting Information). Contrary unique distinct bands at 627, 639, and 1009 cm^{-1} indicating LEC/LEMC and characteristic EtPFPN bands (11 bands) for the STD-FEC-EtPFPN electrolyte formulation have been observed on the anode surface during the SEI formation (Figure 9; Table S1, Supporting Information). One would expect more EtPFPN and LEC/LEMC bands in the in situ Raman measurements of the anode surface for the STD-EtPFPN formulation since the EtPFPN-LEMC species have been confirmed via GC-MS/GC-HRMS measurements (Figures 3 and 4).

As previously mentioned, it is likely that EtPFPN decomposition products (i.e., EtPFPN-LEMC) in the single additive electrolyte blend (STD-EtPFPN) deposit without clinging effectively on the negative electrode surface during the SEI formation process. Thus, these participate beneficially in the SEI formation and improve the electrochemical performance in SiO_x/C anode-based LIBs.

This assumption can now be confirmed with the in situ SHINERS measurements by comparing the bands of the STD-EtPFPN electrolyte blend with the STD-FEC-EtPFPN electrolyte blend in Figure 9. The difference between both electrolyte formulations is only FEC as an additional additive constituent. Additionally, in Tables S1 and S2 (Supporting Information), in situ Raman bands of both electrolyte blends are assigned. It can be observed that the EtPFPN additive cannot cling sufficiently on the negative electrode surface without FEC. Otherwise, more EtPFPN-related bands for the STD-EtPFPN electrolyte blend in Table S2 (Supporting Information) would be observed. Thus, FEC acts like a kit, enabling a second sub-sufficient SEI-forming additive compound like EtPFPN to participate in the SEI formation more effectively with a beneficial output regarding the negative electrode passivation. Hence, a molecular cling effect (MCE) of FEC for a second sub-sufficient additive compound can be postulated according to the observed data, respectively.

Considering our previous study, this observation via GC-MS, GC-HRMS, and in situ SHINERS measurements agrees with the electrochemical cycling data and the gas evolution investigations.^[5,7] According to the results, it is assumed that EtPFPN intervenes right after the EC decomposition at the anode side and therefore terminates the reaction to OHCs. As a consequence, further parasitic reactions leading to gas formation have been inhibited (Figure 5A).^[6] Interestingly, the notable distinct bands at 627, 639, and 1009 cm^{-1} in the SHINERS measurements, which represent LEC/LEMC, were only observed for the STD-FEC-EtPFPN electrolyte blend as distinct bands and not for the other three electrolyte formulations (STD, STD-FEC, STD-EtPFPN) (Table S1, Supporting Information). The assumption condenses that these distinct bands belong to the EtPFPN-LEMC compound, which has been detected via GC-MS/GC-HRMS (Figures 3 and 4). Furthermore, as expected, DEDOHC

Raman bands have been observed for the STD-FEC electrolyte blend at 1030 cm^{-1} . This observation agrees with the literature and the proposed reaction mechanism in Figure 5A (crossed-out blue arrow reaction path).^[6,9,13] Since FEC can only reduce the EC decomposition but not entirely prevent it, one can assume OHC formation according to the EC decomposition pathway mentioned by Gachot et al.^[9] and Henschel et al.^[6] Additionally, this observation underpins the postulated reaction mechanism that EtPFPN intervenes right after the LEMC formation as described in the scheme in Figure 5A, thus, preventing the further reaction of the LEMC species to OHCs by forming the EtPFPN-LEMC species via the proposed transition state. Comparing the STD-FEC-EtPFPN in situ SHINER spectra with the STD-FEC spectra, one can see the lack of distinct bands at 627, 639, and 1009 cm^{-1} and the bands which can be attributed to EtPFPN deposition in the latter spectra (Tables S1 and S3, Supporting Information). On the flip side, according to the GC-HRMS results, one can assume that these bands at 627, 639, and 1009 cm^{-1} can be attributed to the EtPFPN-LEMC compound, which only appears in the presence of FEC in the dual-additive electrolyte approach STD-FEC-EtPFPN. Thus, the EtPFPN-LEMC species could be confirmed indirectly on the negative electrode surface via in situ SHINERS measurements. Considering all these aspects from the GC-MS, GC-HRMS, and the SHINERS measurements, the role of FEC becomes more important as expected; i) FEC is important as robust SEI forming additive as already known from the literature^[21,51–53] and ii) as a new feature have been confirmed, that the MCE of FEC enables a second sub-sufficient SEI forming additive compound to cling on the negative electrode surface and therefore participating effectively in the SEI formation; thus, enabling to improve the SEI efficiency in SiO_x/C based anode materials.

Comparing the in situ SEI surface measurements of the four different electrolyte blends, a different SEI composition morphology has been observed, dependent on the used electrolyte formulation. As expected, the baseline STD electrolyte blend with no electrolyte additive compounds shows more organic interphase, as bands mainly assigned to EC decomposition products have been detected. Additionally, bands indicating Li_2CO_3 and Li_2O_2 are only observed in the baseline electrolyte spectra (Table S4, Supporting Information).

Furthermore, as expected, DEDOHC bands at 474 and 1030 cm^{-1} have been observed for the STD electrolyte blend and the STD-FEC blend since no additive compound can inhibit the initiation, elongation, and termination reaction leading to the formation of OHCs.^[6,9] On the flip side, no OHC bands have been observed for the additive-containing electrolyte blends (STD-EtPFPN, STD-FEC-EtPFPN) in the SHINERS measurements. It is worth mentioning that both additives, FEC and EtPFPN, can reduce the OHC formation (Figure 3).^[5] FEC reduces the OHC formation by preventing the EC decomposition during the SEI formation,^[5] while the EtPFPN intervenes after the EC decomposition, reacting with LEMC to form the EtPFPN-LEMC species and terminating the further reaction process which would lead to OHC formation (Figure 5A). Therefore, it can be assumed that FEC and EtPFPN complement each other in the STD-FEC-EtPFPN electrolyte blend and minimize the OHC formation notably. According to the cell polarization plot in Figure 1 and the homogenous surface morphology observed in the SEM images after SEI formation in Figure 2, one can

assume that lower OHC formation leads to less deposition products on the negative electrode surface and, thus, reduced cell polarization. Since LEMC is an intermediate product in a dynamic reaction process, which reacts immediately further, it is not tangible for analytic measurements. Nevertheless, the final products after several reaction steps can be detected via post-mortem investigations. However, since EtPFPN intervenes right after LEMC formation to the stable EtPFPN-LEMC species, as proposed in Figure 5A, it can be detected via GC-HRMS (Figure 4,1c) and via in situ SHINERS measurements of the negative electrode surface (Table S1, Supporting Information). Here, LEMC becomes more tangible for post-mortem investigations and this enables a better understanding of the dynamic reaction processes during SEI formation. Furthermore, the evaluation of the STD-EtPFPN electrolyte blend shows an organic interphase character with EC decomposition products as SEI components (Table S2, Supporting Information). Conversely, the dual-additive approach STD-FEC-EtPFPN displays an inorganic interphase with a high composition of EtPFPN deposition products on the SEI surface and only traces of EC decomposition products. This confirms the GC-MS measurements in Figure 3, where a reduced EC decomposition for the STD-FEC-EtPFPN blend has been observed upon SEI formation.

3. Conclusion

In this work, the SEI formation on SiO_x/C anodes in the presence of a baseline electrolyte environment (LiPF_6 in EC/EMC 3:7 by wt.) with FEC and/or EtPFPN as SEI film-forming additives has been investigated, and insights into the synergistic effect of the dual-additive electrolyte approach (STD-FEC-EtPFPN) have been presented and thoroughly discussed in terms of beneficial aspects for LIBs cell performance compared to state-of-the-art electrolyte formulations (STD-FEC). This dual-additive approach results in an effective electrolyte formulation with the property to reduce notably the electrochemical EC decomposition during the SEI formation. Additionally, this approach intervenes in secondary reactions to form EtPFPN-LEMC species once EC decomposition takes place, leading to reduced side reactions during the cell operation, improved electrolyte stability, and better electrochemical performance.^[6,9,13] The interplay between EC, Li-alkoxide, LEMC, FEC, and EtPFPN has been visualized schematically via a reaction mechanism postulated based on analytical data of the electrolyte via GC-MS/GC-HRMS and in situ SHINERS measurements of the SEI. Furthermore, a novel property of FEC is characterized within these measurements, called molecular-cling-effect (MCE). According to the measured data, one can assume that FEC has an MCE on sub-sufficient SEI forming additive compounds, which enables these sub-sufficient additive compounds to participate effectively in the SEI formation, improving the SEI formation notably without a negative effect for the bulk solvent and the electrochemical performance. Currently, there is no comparative enhancing effect for FEC mentioned in the literature. Hence, this effect of FEC enables improved SEI formation in LIB cells and opens a new perspective for SEI sub-sufficient additive compounds, which have not been considered in the past due to ineffective passivation, and therefore low SEI forming properties.

4. Experimental Section

Pouch Cell Setup: Nominally identical, machine-made wound pouch cells (≈ 200 mAh capacity, voltage window 2.8 – 4.3 V) were obtained from Li-Fun Technology. If not otherwise stated, all these cells were composed of $\text{LiNi}_{0.5}\text{Co}_{0.2}\text{Mn}_{0.3}\text{O}_2$ (NCM523) positive electrodes and SiO_x/C negative electrodes. Details of the electrodes are provided in Table 1. Both sides of the electrodes were coated, except for small regions on one side at the end of the foils. The pouch cells were pre-dried in an oven at 80 °C under reduced pressure ($< 10^{-3}$ bar) for 24 h in a dry room (dew point, -80 °C; < 0.55 ppm water). After the pre-drying process, the cells were filled with 0.75 mL (≈ 0.90 g $\pm 1\%$) electrolyte and vacuum-sealed by heat-crimping at 165 °C for 5 s at a relative pressure of -87 kPa using a vacuum sealer (GN-HS200V, Gelon LIB Group). Custom cell holders with reproducible pressure (2 bar) on the cell stack were used to clamp the cells.^[30] A calibrated torque screwdriver was used to fix the custom cell holders and to maintain a pressure of 2 bar.

Electrolyte Compositions: The baseline electrolyte (referred to as STD) contained 1 M LiPF_6 in a solution of 3:7 (by weight) ethylene carbonate: ethyl methyl carbonate (EC:EMC; E-Lyte Innovations, battery grade). As a benchmark electrolyte additive, 2.0 wt.% FEC (BASF, 98.7% pure), corresponding to 188.59 μmol FEC in 1 g STD electrolyte, was used. The same molal value of FEC (188.59 μmol) was used to calculate the mass of the ethoxy-(pentafluoro)-cyclotriphosphazene (EtPFPN, TCI Chemicals, 98.0% pure) compound to ensure the same molal concentration with FEC in all single- and dual-additive electrolytes. For the single-additive electrolyte, three cells for each sample were filled with 0.75 mL ± 1 wt.% of the STD electrolyte, containing LiPF_6 salt in a solution of 3:7 (by weight) EC:EMC with 188.59 μmol of the additives FEC or EtPFPN. For the dual-additive electrolyte, three cells for each sample were filled with 0.75 mL ± 1 wt.% of the STD electrolyte containing LiPF_6 salt in a solution of 3:7 (by weight) EC:EMC with a 1:1 (molal ratio) of FEC and EtPFPN. All chemical compounds were used as derived from the supplier without further purification. The STD electrolyte was prepared in a glovebox (O_2 , H_2O < 0.1 ppm), transferred in a vacuum-sealed device to the dry room (dew point, -80 °C; < 0.55 ppm water) where the additives were added, and the pouch cells were filled with the electrolyte blends. Details of each additive are provided in Table 2.

Electrochemical Cycling Procedure at 20 °C: After filling the pouch cells with electrolyte and after vacuum sealing, they were connected to the battery and cell test equipment with a temperature chamber controlled at 20 °C ± 0.1 °C from MACCOR Inc. For SEI formation, the pouch cells were held at 1.0 V for 20 h, charged to 3.5 V at 10 mA (≈ 0.05 C), followed by a constant voltage (CV) step for 1 h and continued with a discharge to 2.8 V at 10 mA (≈ 0.05 C). The cells were then charged two times to the upper-cut voltage of 4.3 V at 40 mA (≈ 0.2 C), at the top of charge (upper-cut voltage), CV was held after each charging process until the current dropped below 4 mA (≈ 0.02 C) to initiate the discharge process to the lower-cut voltage 2.8 V.^[5] Afterward, the cells were transferred to the dry room, de-gassed, and vacuum-sealed again at the discharged state. For long-term cycling, the pouch cells were charged/discharged between 2.8 V – 4.3 V at 100 mA (≈ 0.5 C) for 200 cycles, if not otherwise stated.

Negative Electrode Preparation for the SHINERS Measurements: Composite electrodes (SiO_x/C) were designed to consist of 85 wt.% active material, 5 wt.% conductive carbon (Super C65, carbon black, Imerys, battery grade), and 10 wt.% binders comprising 7.7 wt.% sodium-carboxymethyl cellulose (Na-CMC, Walocel CRT 2000 PPA 12, Dow Wolff Cellulosics, battery grade) and 2.3 wt.% polyacrylic acids (PAA, Sigma-Aldrich, purity 99.0%). The active material made up of 10 wt.% SiO_x (average particle size 4 μm , Wacker Chemie AG, battery grade) and 90 wt.% graphite (SMG A5, Hitachi, battery grade). SiO_x/C composites were obtained by grounding SiO_x and graphite in a mortar. For the electrode paste preparation, the binder was added together with 1.3 wt.% of lithium hydroxide (LiOH , Sigma-Aldrich, purity 99.0%) to 70 wt.% de-ionized water and mixed at 1700 rpm for 20 min (Planetary Centrifugal Mixer, THINKY MIXER ARE-310, Thinky Corporation). After homogenization, active material and conductive agent were added, and the electrode paste was mixed for another 40 min. The coating was cast at a speed of 50 mm s⁻¹ using a standard

Table 1. Electrode composition of NCM523 || SiO_x/C pouch cells with a PE one-side coated Al₂O₃ separator.

	Positive Electrode	Negative Electrode
Active material	NCM523 94 wt. %	Artificial graphite (90 wt. %) and SiO _x (10 wt. %) [85.32 wt. % 9.48 wt. %]
Conductive agent	Carbon black, 4 wt. %	Carbon black (1.4 wt. %)
Binder	PVdF, 2 wt. %	CMC and SBR [1.3 wt. % 2.5 wt. %]
Mass loading	16.5 mg cm ⁻²	8 mg cm ⁻²
Balanced at cut-off voltage		4.3 V

Table 2. Composition of the single additive and dual-additive blends in the STD electrolyte.

Electrolyte Additive	FEC	EtPFPN
Molecular weight g mol ⁻¹	106.05	275.00
Moles μmol ⁻¹	188.59	188.59
Mass per gram electrolyte mg ⁻¹	20.00	51.86
Single-additive	FEC	EthoxyPFPN
Dual-additive 1:1 (molal ratio)	-	FEC: EthoxyPFPN

doctor-blade technique (ZUA 2000 Universal Applicator, Zehntner GmbH) and (Automatic Film Applicator 1133N, TQC Sheen) applying a gap of 120 μm (wet film thickness) onto the copper foil (Schlenk Metallfolien GmbH & Co. KG). The first drying procedure was performed in a laboratory oven at 80 °C for 24 h (dry film thickness 94 μm). Afterward, the electrodes were punched out with a disc diameter of Ø = 15 mm (Hohsen, electrode punch). The punched electrodes were dried again in a vacuum drying oven (Büchi Glass Oven B-585, Büchi Labortechnik GmbH) at 120 °C under reduced pressure (<0.05 mbar) for 12 h to remove residual water. After the drying procedure, the electrodes were transferred in a vacuum-sealed device to the dry room (dew point, -80 °C; < 0.55 ppm water), where they were first weighed with an analytical balance (ME-235S, Sartorius, accuracy of ± 0.01 mg) and then stored vacuum sealed in the dry room. The mass loading of all electrodes was ≈ 2.4 ± 0.3 mg cm⁻² (average areal capacity ≈ 1.35 ± 0.1 mAh cm⁻²).

Positive Electrode Preparation for the SHINERS Measurements: Cathode samples LiNi_{0.6}Co_{0.2}Mn_{0.2}O₂ (NCM622) were prepared on a large scale at an in-house pilot plant battery production line. The respective active material and inactive components are summarized in **Table 3**. The cathode consisted of 95 wt. % NCM622 (polycrystalline), 3 wt. % polyvinylidene

difluoride (PVDF) binder, and 2 wt. % carbon black and were cast onto aluminum foil as a current collector using *N*-methyl-2-pyrrolidone as solvent. After drying at 100 °C for 12 h (30% porosity) and calendaring (55 t, 5 min, thickness before calendaring 47 μm, after calendaring 39 μm) the electrode sheets were punched into electrode discs (Ø 14 mm) in dry room (dew point, -80 °C; < 0.55 ppm water) and were dried at reduced pressure (< 10⁻³ mbar) and 90 °C for 20 h.

Nanoparticle Preparation: For the SHINERS investigations,^[54] SiO_x-coated Au-NPs were synthesized. 100 mL of 0.01 wt. %/vol AuCl₃ (99.995 %, Sigma Aldrich) solution was added to a round bottom flask and brought to a boil. 0.7 mL of a 1 wt. % sodium citrate solution (reference standard, USP) was added to the boiling solution, and the mixture was stirred for 30 min under reflux to obtain Au-NPs. For the SiO_x coating, 30 mL of the Au-NP solution was added into a round bottom flask. Under vigorous stirring, 0.4 mL of a 1.0 mM 3-aminopropyltrimethoxysilane solution (APTMS, 97 %, Sigma Aldrich) was added, and the mixture was stirred for 15 minutes at room temperature. Afterward, 2.4 mL of a 0.54 wt. % sodium trisilicate solution (reagent grade, Sigma Aldrich) (pH = 10; adjusted with HCl) was added, and the mixture was heated to 90 °C. After stirring for 60 min, the mixture was cooled in an ice bath. To wash the coated NPs, the mixture was centrifuged at 4500 rpm for 10 min. The supernatant was removed and replaced with water (SiO_x-Au-NPs size 49 nm ± 5 nm). The washing step was repeated twice. All used glassware was cleaned with aqua regia (HNO₃/HCl, 3:1 by volume) beforehand. For the preparation of the solutions and washing of the NPs, only MilliQ-water (Merck, 18.2 MΩ cm⁻¹) was used. To ensure a complete coating, a 10 mM pyridine solution was added to the NPs. In the case of an incomplete coating, pyridine coordination with the gold particle accessed in the coating pinholes of the NPs shows characteristic peaks at 1012 and 1037 cm⁻¹ (Figure S4, Supporting Information). Those peaks were not observed for the coated NPs used here in this study. SEM measurements of the SiO_x-Au-NPs are provided in Figure S5A,B (Supporting Information).

Sample Preparation for Raman Spectroscopy Measurements: To apply the SiO_x-Au-NPs to the electrode surface, the NPs were transferred to isopropanol before application. The aqueous solution was centrifuged for 10 min at 4500 rpm, the supernatant was decanted and replaced with isopropanol before, and the emerging solution was centrifuged again. Two-thirds of the supernatant was removed, and 60 μL of the residual, concentrated NP suspension was added to the investigated dry electrode surface (Figure S6). The solvent was evaporated, and another 40 μL of the NP suspension was added. The solvent was evaporated, and the electrode was dried at 60 °C for at least 2 h in a vacuum drying oven. Raman spectroscopy was conducted in an air-tight optical cell (EL-CELL ECC-Opto-Std) using an NCM622 || SiO_x/C two-electrode full-cell setup. In the chosen setup, both electrodes had their active material facing the glass window and were separated by one layer of Celgard 2500. A copper mesh was placed above the SiO_x/C electrode to ensure sufficient diffusion over the sides. For electrochemical aging, three CV-cycles in a voltage range between 2.8 and 4.3 V with a scan rate of 150 μV s⁻¹ were performed using an Autolab Battery Tester (Metrohm) controlled by NOVA 2.1 (Autolab) software.

Raman Spectroscopy Investigations: A Horiba Scientific confocal Raman microscope (LabRAM HR evolution, air-cooled CCD detector) was

Table 3. Materials and chemicals for composite electrode preparation.

	NCM622 Electrode
Material	NCM622 95 wt. %
Conductive Carbon	SuperC65 2 wt. %
Binder 1	PVDF 3 wt. %
Theo. Geo. Cap.	1.15 mAh cm ⁻²
Mass loading	6.7 mg cm ⁻²
Dry film thickness	21 μm
Porosity	30%
Aluminum current collector	15 μm
MEET Batch No.	345

used to investigate the SEI surface. The sample was excited with a green laser with a wavelength of 532 nm and 12.2 mW output power at the sample, adjusted by a 5% filter to 0.61 mW with a 600 line/mm grating. The beam was focused using a magnification distance objective (50× long-working distance objective, Carl Zeiss Microscopy, 9.2 mm, numerical aperture 0.5). Raman spectra were collected by two integrations of 50 s each. Handling the Raman microscope, collecting the spectra, and evaluating the data were done using LabSpec6.6.2 (Horiba Scientific). Prior to the measurement, the system was calibrated on the silicon peak at a Raman shift of 520.7 cm^{-1} .

Gas Chromatography-Mass Spectrometry: The aged electrolyte after the SEI formation at 20 °C was investigated. For that, the pouch cells were opened in a glovebox (O_2 , H_2O contents <0.1 ppm), and the electrolytes were extracted via centrifugation of the separator stack. Afterward, electrolyte samples were diluted at 1:100 with DMC prior to measurements to precipitate the conducting salt. Gas chromatography-mass spectrometry (GC-MS) experiments were performed on a Shimadzu GCMS-QP2010 Ultra device with assembled AOC-5000 Plus autosampler and a nonpolar Supelco SLB®–5 ms (30m × 0.25 mm, 0.25 μm ; Sigma Aldrich) column. Further parameters and sample preparation conditions were applied according to Grütze and Mönninghoff et al.^[55,56]

Gas Chromatography High Resolution-Accurate Mass Spectrometry: GC investigations with high resolution-accurate mass spectrometry (HRMS) detection were performed on a Q Exactive GC Orbitrap GC-MS/MS system with a TRACE 1310 GC and a TriPlus RSH autosampler (all Thermo Fisher Scientific, USA). The MS resolution was set to 60 000 (full width at half maximum (FWHM) at m/z 200). Chromatographic separation was obtained with the same parameters as for the quadrupole-MS experiments. Chemical ionization was performed with ammonia (3.5 purity, Westfalen, Germany). Detailed experimental parameters were applied according to Peschel et al.^[10,57] and non-target analysis was performed based on extracted ion chromatograms (EICs) of measured accurate masses with a mass window of 5 ppm.

Density Functional Theory Calculations: The initial geometries were generated by the CREST tool,^[42] which provided a set of low-energy structures at the GFN2-xTB level of theory^[43] that were not higher than 6 kcal mol^{-1} in energy with respect to the lowest-energy geometry. Subsequently, these structures were reoptimized at the $\omega\text{B97X-D3/def2-TZVP}$ level of theory^[38–41] with the Gaussian 16 software (Gaussian 16, Revision B.01, M. J. Frisch, G. W. Trucks, H. B. Schlegel, G. E. Scuseria, M. A. Robb, J. R. Cheeseman, G. Scalmani, V. Barone, G. A. Petersson, H. Nakatsuji, X. Li, M. Caricato, A. V. Marenich, J. Bloino, B. G. Janesko, R. Gomperts, B. Mennucci, H. P. Hratchian, J. V. Ortiz, A. F. Izmaylov, J. L. Sonnenberg, D. Williams-Young, F. Ding, F. Lipparini, F. Egidi, J. Goings, B. Peng, A. Petrone, T. Henderson, D. Ranasinghe, V. G. Zakrzewski, J. Gao, N. Rega, G. Zheng, W. Liang, M. Hada, M. Ehara, K. Toyota, R. Fukuda, J. Hasegawa, M. Ishida, T. Nakajima, Y. Honda, O. Kitao, H. Nakai, T. Vreven, K. Throssell, J. A. Montgomery, Jr., J. E. Peralta, F. Ogliaro, M. J. Bearpark, J. J. Heyd, E. N. Brothers, K. N. Kudin, V. N. Staroverov, T. A. Keith, R. Kobayashi, J. Normand, K. Raghavachari, A. P. Rendell, J. C. Burant, S. S. Iyengar, J. Tomasi, M. Cossi, J. M. Millam, M. Klene, C. Adamo, R. Cammi, J. W. Ochterski, R. L. Martin, K. Morokuma, O. Farkas, J. B. Foresman, and D. J. Fox, Gaussian Inc., Wallingford CT, 2016). All calculations were performed with the SMD implicit solvation model^[58] at 298 K with built-in parameters for acetone, which has a similar dielectric constant as the carbonate blends used for electrolytes.^[59,60]

Scanning Electron Microscopy Analysis of SiO_x/C Anodes: The negative electrodes were analyzed via SEM before cycling (pristine) and after the SEI formation. Cells ($\text{LiNi}_{0.5}\text{Co}_{0.2}\text{Mn}_{0.3}\text{O}$ (NCM523) || SiO_x/C) were opened after cycling in an argon-filled glovebox (O_2 , H_2O contents < 0.1 ppm). The SiO_x/C anodes were extracted and rinsed three times with dimethyl carbonate (DMC; BASF, battery grade) to remove electrolyte salt residues. At least three cells were investigated for each electrolyte formulation to ensure high reproducibility. Samples were placed on a vacuum-sealed sample holder and transferred to the SEM chamber without exposure to ambient air. To investigate the SiO_x/C electrode surface morphology of pristine and aged anodes, a scanning electron microscope (SEM, Carl-Zeiss Cross-Beam 550, Carl Zeiss Microscopy GmbH) equipped with a field emission

gun (Schottky-type) and an in-lens secondary electron detector was used. The working distance for the SEM images was 5.1 mm with an accelerating voltage of 3.5 kV. Energy dispersion X-ray spectroscopy (EDX) at an acceleration voltage of 3.5 kV was measured with an Ultim Extrem detector (Oxford Instruments). To evaluate the elemental composition of the samples, AZtech software (Oxford Instruments) was used.

Supporting Information

Supporting Information is available from the Wiley Online Library or from the author.

Acknowledgements

The authors wish to thank the Ministry of Economy, Innovation, Digitalization and Energy of North-Rhine Westphalia for funding this work in the project “GrEEn” (313-W044A). The work of Masoud Baghernejad, Felix Pfeiffer, and Matthias Weiling has been supported by the German Federal Ministry for Education and Research within the project “EFoBatt” grant number 13XP5129.

Open access funding enabled and organized by Projekt DEAL.

Conflict of Interest

The authors declare no conflict of interest.

Data Availability Statement

The data that support the findings of this study are available from the corresponding author upon reasonable request.

Keywords

lithium-ion batteries, phosphazene compounds, Raman spectroscopy, silicon anodes, solid electrolyte interphases

Received: March 23, 2023

Revised: June 20, 2023

Published online: July 4, 2023

- [1] D. R. Gallus, R. Wagner, S. Wiemers-Meyer, M. Winter, I. Cekic-Laskovic, *Electrochim. Acta* **2015**, *184*, 410.
- [2] M. Börner, F. Horsthemke, F. Kollmer, S. Haseloff, A. Friesen, P. Niehoff, S. Nowak, M. Winter, F. M. Schappacher, *J. Power Sources* **2016**, *335*, 45.
- [3] Q. Liu, Z. Chen, Y. Liu, Y. Hong, W. Wang, J. Wang, B. Zhao, Y. Xu, J. Wang, X. Fan, L. Li, H. bin Wu, *Energy Storage Mater.* **2021**, *37*, 521.
- [4] J. Liu, X. Song, L. Zhou, S. Wang, W. Song, W. Liu, H. Long, L. Zhou, H. Wu, C. Feng, Z. Guo, *Nano Energy* **2018**, *46*, 404.
- [5] A. Ghaur, C. Peschel, I. Dienwiebel, L. Haneke, L. Du, L. Profanter, A. Gomez-Martin, M. Winter, S. Nowak, T. Placke, *Adv. Energy Mater.* **2023**, 2203503.
- [6] J. Henschel, C. Peschel, S. Klein, F. Horsthemke, M. Winter, S. Nowak, *Angew. Chem., Int. Ed.* **2020**, *59*, 6128.
- [7] H. Yoshida, T. Fukunaga, T. Hazama, M. Terasaki, M. Mizutani, M. Yamachi, *J. Power Sources* **1997**, *68*, 311.
- [8] F. Shi, H. Zhao, G. Liu, P. N. Ross, G. A. Somorjai, K. Komvopoulos, *J. Phys. Chem. C* **2014**, *118*, 14732.

- [9] G. Gachot, S. Grugeon, M. Armand, S. Pilard, P. Guenot, J.-M. Tarascon, S. Laruelle, *J. Power Sources* **2008**, 178, 409.
- [10] C. Peschel, F. Horsthemke, M. Winter, S. Nowak, *MethodsX* **2022**, 9, 101621.
- [11] Z. X. Shu, R. S. McMillan, J. J. Murray, *J. Electrochem. Soc.* **1993**, 140, 922.
- [12] L. M. Thompson, W. Stone, A. Eldesoky, N. K. Smith, C. R. M. McFarlane, J. S. Kim, M. B. Johnson, R. Petibon, J. R. Dahn, *J. Electrochem. Soc.* **2018**, 165, A2732.
- [13] L. Wang, A. Menakath, F. Han, Y. Wang, P. Y. Zavalij, K. J. Gaskell, O. Borodin, D. Iuga, S. P. Brown, C. Wang, K. Xu, B. W. Eichhorn, *Nat. Chem.* **2019**, 11, 789.
- [14] S. K. Heiskanen, J. Kim, B. L. Lucht, *Joule* **2019**, 3, 2322.
- [15] M.-H. Ryou, J.-N. Lee, D. J. Lee, W.-K. Kim, Y. K. Jeong, J. W. Choi, J.-K. Park, Y. M. Lee, *Electrochim. Acta* **2012**, 83, 259.
- [16] L. Cabo-Fernandez, D. Bresser, F. Braga, S. Passerini, L. J. Hardwick, *Batter Supercaps* **2019**, 2, 168.
- [17] H. Li, Y. Mo, N. Pei, X. Xu, X. Huang, L. Chen, *J. Phys. Chem. B* **2000**, 104, 8477.
- [18] R. Schmitz, R. Ansgar Müller, R. Wilhelm Schmitz, C. Schreiner, M. Kunze, A. Lex-Balducci, S. Passerini, M. Winter, *J. Power Sources* **2013**, 233, 110.
- [19] L. Ma, L. Ellis, S. L. Glazier, X. Ma, Q. Liu, J. Li, J. R. Dahn, *J. Electrochem. Soc.* **2018**, 165, A891.
- [20] J. Kasnatscheew, M. Evertz, B. Streipert, R. Wagner, R. Klöpsch, B. Vortmann, H. Hahn, S. Nowak, M. Amereller, A.-C. Gentschev, P. Lamp, M. Winter, *Phys. Chem. Chem. Phys.* **2016**, 18, 3956.
- [21] T. Jaumann, J. Balach, M. Klose, S. Oswald, U. Langklotz, A. Michaelis, J. Eckert, L. Giebeler, *Phys. Chem. Chem. Phys.* **2015**, 17, 24956.
- [22] A. Wang, S. Kadam, H. Li, S. Shi, Y. Qi, *NPJ Comput Mater* **2018**, 4, 15.
- [23] H. Adenusi, G. A. Chass, S. Passerini, K. v. Tian, G. Chen, *Adv. Energy Mater.* **2023**, 13, 2203307.
- [24] R. Jung, M. Metzger, D. Haering, S. Solchenbach, C. Marino, N. Tsiouvaras, C. Stinner, H. A. Gasteiger, *J. Electrochem. Soc.* **2016**, 163, A1705.
- [25] C. P. Aiken, J. Xia, D. Y. Wang, D. A. Stevens, S. Trussler, J. R. Dahn, *J. Electrochem. Soc.* **2014**, 161, A1548.
- [26] L. D. Ellis, J. P. Allen, L. M. Thompson, J. E. Harlow, W. J. Stone, I. G. Hill, J. R. Dahn, *J. Electrochem. Soc.* **2017**, 164, A3518.
- [27] K. Xu, Y. Lam, S. S. Zhang, T. R. Jow, T. B. Curtis, *J. Phys. Chem. C* **2007**, 111, 7411.
- [28] G. v. Zhuang, K. Xu, H. Yang, T. R. Jow, P. N. Ross, *J. Phys. Chem. B* **2005**, 109, 17567.
- [29] E. Markevich, G. Salitra, D. Aurbach, *ACS Energy Lett.* **2017**, 2, 1337.
- [30] J.-P. Schmiegél, R. Nölle, J. Henschel, L. Quach, S. Nowak, M. Winter, F. Glorius, T. Placke, *Cell Rep Phys Sci* **2021**, 2, 100327.
- [31] R. Nölle, J.-P. Schmiegél, M. Winter, T. Placke, *Chem. Mater.* **2020**, 32, 173.
- [32] Y.-H. Liu, M. Okano, T. Mukai, K. Inoue, M. Yanagida, T. Sakai, *J. Power Sources* **2016**, 304, 9.
- [33] C. K. Chan, H. Peng, G. Liu, K. McIlwrath, X. F. Zhang, R. A. Huggins, Y. Cui, *Nat. Nanotechnol.* **2008**, 3, 31.
- [34] S. K. Soni, B. W. Sheldon, X. Xiao, M. W. Verbrugge, A. Dongjoon, H. H., G. Huajian, *J. Electrochem. Soc.* **2011**, 159, A38.
- [35] T. A. Luther, F. F. Stewart, J. L. Budzien, R. A. LaViolette, W. F. Bauer, M. K. Harrup, C. W. Allen, A. Elayan, *J. Phys. Chem. B* **2003**, 107, 3168.
- [36] M. T. Benson, M. K. Harrup, K. L. Gering, *Comput. Theor. Chem.* **2013**, 1005, 25.
- [37] T. T. K. Ingber, D. Liebenau, M. Biedermann, M. Kolek, D. Diddens, H.-D. Wiemhöfer, A. Heuer, M. Winter, P. Bieker, *J. Electrochem. Soc.* **2021**, 168, 070559.
- [38] J.-D. Chai, M. Head-Gordon, *Phys. Chem. Chem. Phys.* **2008**, 10, 6615.
- [39] F. Weigend, R. Ahlrichs, *Phys. Chem. Chem. Phys.* **2005**, 7, 3297.
- [40] F. Weigend, *Phys. Chem. Chem. Phys.* **2006**, 8, 1057.
- [41] S. Grimme, J. Antony, S. Ehrlich, H. Krieg, *J. Chem. Phys.* **2010**, 132, 154104.
- [42] P. Pracht, F. Bohle, S. Grimme, *Phys. Chem. Chem. Phys.* **2020**, 22, 7169.
- [43] C. Bannwarth, S. Ehlert, S. Grimme, *J. Chem. Theory Comput.* **2019**, 15, 1652.
- [44] M. Weiling, F. Pfeiffer, M. Baghernejad, *Adv. Energy Mater.* **2022**, 12, 2202504.
- [45] F. Pfeiffer, D. Diddens, M. Weiling, M. Baghernejad, *ACS Appl. Mater. Interfaces* **2023**, 15, 6676.
- [46] F. Pfeiffer, D. Diddens, M. Weiling, L. Frankenstein, S. Kühn, I. Cekic-Laskovic, M. Baghernejad, *Adv. Energy Mater.* **2023**, 202300827.
- [47] J. R. Menendez, G. A. Carriedo, F. J. Garcia-Alonso, E. Clavijo, M. Nazri, R. Aroca, *J. Raman Spectrosc.* **1999**, 30, 1121.
- [48] G. A. Carriedo, F. J. García Alonso, P. A. González, J. R. Menéndez, *J. Raman Spectrosc.* **1998**, 29, 327.
- [49] A. Gajan, C. Lecourt, B. E. Torres Bautista, L. Fillaud, J. Demeaux, I. T. Lucas, *ACS Energy Lett.* **2021**, 6, 1757.
- [50] K. Xu, A. von Cresce, *J. Mater. Chem.* **2011**, 21, 9849.
- [51] K. U. Schwenke, S. Solchenbach, J. Demeaux, B. L. Lucht, H. A. Gasteiger, *J. Electrochem. Soc.* **2019**, 166, A2035.
- [52] F. Lindgren, C. Xu, L. Niedzicki, M. Marcinek, T. Gustafsson, F. Björefors, K. Edström, R. Younesi, *ACS Appl. Mater. Interfaces* **2016**, 8, 15758.
- [53] M. Winter, *Zeitschrift für Physikalische Chemie* **2009**, 223, 1395.
- [54] J. F. Li, X. D. Tian, S. B. Li, J. R. Anema, Z. L. Yang, Y. Ding, Y. F. Wu, Y. M. Zeng, Q. Z. Chen, B. Ren, Z. L. Wang, Z. Q. Tian, *Nat. Protoc.* **2013**, 8, 52.
- [55] M. Grütze, X. Mönnighoff, F. Horsthemke, V. Kraft, M. Winter, S. Nowak, *RSC Adv.* **2015**, 5, 43209.
- [56] X. Mönnighoff, A. Friesen, B. Konersmann, F. Horsthemke, M. Grütze, M. Winter, S. Nowak, *J. Power Sources* **2017**, 352, 56.
- [57] C. Peschel, S. Nowak, D. Roberts, in *Thermo Fisher Technical Note 00413*, Thermo Fisher Scientific, Waltham, USA **2022**.
- [58] A. v. Marenich, C. J. Cramer, D. G. Truhlar, *J. Phys. Chem. B* **2009**, 113, 6378.
- [59] O. Borodin, M. Olguin, C. E. Spear, K. W. Leiter, J. Knap, *Nanotechnology* **2015**, 26, 354003.
- [60] D. S. Hall, J. Self, J. R. Dahn, *J. Phys. Chem. C* **2015**, 119, 22322.